Measurement of the $e^+e^- \to \eta\pi^+\pi^-$ cross section in the center-of-mass energy range 1.22–2.00 GeV with the SND detector at the VEPP-2000 collider

V. M. Aulchenko,[1] M. N. Achasov,[1,2] A. Yu. Barnyakov,[1] K. I. Beloborodov,[1,2] A. V. Berdyugin,[1,2] A. G. Bogdanchikov,[1,2] A. A. Botov,[1] T. V. Dimova,[1,2] V. P. Druzhinin,[1,2] V. B. Golubev,[1,2] L. V. Kardapoltsev,[1,2] A. G. Kharlamov,[1,2] I. A. Koop,[1,2] A. A. Korol,[1,2] S. V. Koshuba,[1] D. P. Kovrizhin,[1] A. S. Kupich,[1,2] K. A. Martin,[1] A. E. Obrazovsky,[1] E. V. Pakhtusova,[1,2] A. I. Senchenko,[1] S. I. Serednyakov,[1] Z. K. Silagadze,[1] Yu. M. Shatunov,[1] P. Ju. Shatunov,[1,2] D. A. Shtol,[1,*] D. B. Shwartz,[1,2] A. N. Skrinsky,[1] I. K. Surin,[1] Yu. A. Tikhonov,[1,2] Yu. V. Usov,[1] and A. V. Vasiljev[1,2]

[1]*Budker Institute of Nuclear Physics, SB RAS, Novosibirsk 630090, Russia*
[2]*Novosibirsk State University, Novosibirsk 630090, Russia*

(Received 8 December 2014; published 18 March 2015)

In the experiment with the SND detector at the VEPP-2000 e^+e^- collider the cross section for the process $e^+e^- \to \eta\pi^+\pi^-$ has been measured in the center-of-mass energy range from 1.22 to 2.00 GeV. Obtained results are in agreement with previous measurements and have better accuracy. The energy dependence of the $e^+e^- \to \eta\pi^+\pi^-$ cross section has been fitted with the vector-meson dominance model. From this fit the product of the branching fractions $B(\rho(1450) \to \eta\pi^+\pi^-)B(\rho(1450) \to e^+e^-)$ has been extracted and compared with the same products for $\rho(1450) \to \omega\pi^0$ and $\rho(1450) \to \pi^+\pi^-$ decays. The obtained cross section data have been also used to test the conservation of vector current hypothesis.

DOI: 10.1103/PhysRevD.91.052013 PACS numbers: 13.66.Bc, 13.25.-k, 14.40.-n

I. INTRODUCTION

The process $e^+e^- \to \eta\pi^+\pi^-$ contributes to the isovector part of the electromagnetic hadronic current. In the vector-meson dominance (VMD) model it is described by the diagram shown in Fig. 1, where V are $\rho(770)$, $\rho(1450)$, and $\rho(1700)$ resonances. In contrast to the main isovector modes $e^+e^- \to \pi^+\pi^-\pi^0\pi^0$ and $\pi^+\pi^-\pi^+\pi^-$ the process $e^+e^- \to \eta\pi^+\pi^-$ is dominated by one intermediate state only, $\eta\rho(770)$, and therefore important for determination of $\rho(1450)$ and $\rho(1700)$ resonance parameters. The process gives a sizable contribution, up to 5% at center-of-mass (c.m.) energy $\sqrt{s} = 1.5$ GeV, to the total hadronic cross section, which is determined below 2 GeV as a sum of exclusive modes. Data on $e^+e^- \to \eta\pi^+\pi^-$ can be used to test the conservation of vector current (CVC) hypothesis, which predicts a relation between the $e^+e^- \to \eta\pi^+\pi^-$ cross section and the spectral function for the $\tau^- \to \eta\pi^-\pi^0\nu_\tau$ decay.

The $e^+e^- \to \eta\pi^+\pi^-$ process was earlier studied in several experiments [1–5]. The most precise measurements were performed at the VEPP-2M e^+e^- collider with the CMD-2 [3] and SND [5] detectors below 1.4 GeV, and at PEP-II B-factory with the *BABAR* detector [4] above 1.4 GeV using the initial state radiation technique. In the CMD-2 and *BABAR* measurements the η meson was reconstructed via its decay to $\pi^+\pi^-\pi^0$, while SND used the $\eta \to \gamma\gamma$ decay mode. This work continues the SND study of Ref. [5] in a wider energy region, up to 2 GeV, using data collected at the VEPP-2000 e^+e^- collider [6].

II. EXPERIMENT

SND is a nonmagnetic detector consisting of a tracking system, aerogel threshold Cherenkov counters for kaon identification, an electromagnetic calorimeter, and a muon system. The tracking system based on a nine-layer drift chamber provides solid angle coverage of 94% of 4π and azimuthal and polar angle resolutions of 0.45° and 0.8°, respectively. The three-layer spherical electromagnetic calorimeter contains 1640 NaI(Tl) crystals with a total thickness of $13.4X_0$, where X_0 is the radiation length. A solid angle covered by the calorimeter is 90% of 4π. Its energy resolution for photons is $\sigma_{E_\gamma}/E_\gamma = 4.2\%\sqrt[4]{E_\gamma(\mathrm{GeV})}$, and the angular resolution about 1.5°.

The experiment was performed at the VEPP-2000 in 2011–2012. The c.m. energy range $\sqrt{s} = 1.05$–2.00 GeV was scanned several times with a step of 25 MeV. The total integrated luminosity collected by SND in this energy range is about 35 pb^{-1}. The analysis was performed initially for 2011 and 2012 data separately. Since the cross

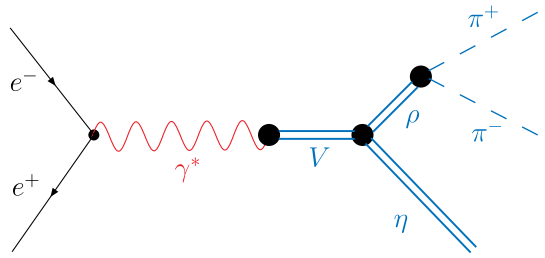

FIG. 1 (color online). The diagram for the process $e^+e^- \to \eta\pi^+\pi^-$ in the VMD model.

*D.A.Shtol@inp.nsk.su

sections measured in the two data sets are found to be consistent, data collected at close energies in 2011 and 2012 are combined in the analysis presented in this paper.

III. EVENT SELECTION

Preliminary selection of $e^+e^- \to \eta\pi^+\pi^-$ ($\eta \to \gamma\gamma$) event candidates is based on the following requirements:

(i) $N_c = 2$, where N_c is the number of charged particles originating from the interaction region. Each charged-particle track must cross at least four drift-chamber layers and has $r_i < 0.3$ cm and $|Z_i| < 10$ cm, where r_i is the distance between the track and the beam axis, and Z_i is the z-coordinate of the track at its distance of the closest approach to the beam axis.

(ii) $N_\gamma = 2$, where N_γ is the number of reconstructed photons. The photon polar angle must be in the range $36° < \theta_\gamma < 144°$.

(iii) $0.4 < E_{\rm tot}/\sqrt{s} < 0.9$ and $E_{\rm char}/\sqrt{s} < 0.65$, where $E_{\rm tot}$ is the total energy deposition in the calorimeter, and $E_{\rm char}$ is the total energy deposition in the calorimeter from charged particles. These conditions suppress QED background.

For selected events we perform a geometrical fit to a common vertex and a two-constrained kinematic fit to the $e^+e^- \to \pi^+\pi^-\gamma\gamma$ hypothesis, and then apply the following additional conditions:

(i) $\chi^2_{\rm vertex} < 200$, where $\chi^2_{\rm vertex}$ is χ^2 of the vertex fit.

(ii) $\chi^2_{\pi^+\pi^-\gamma\gamma} < 60$, where $\chi^2_{\pi^+\pi^-\gamma\gamma}$ is χ^2 of the kinematic fit.

(iii) 400 MeV $\le m_{\gamma\gamma} \le$ 700 MeV, where $m_{\gamma\gamma}$ is the two-photon invariant mass calculated using photon parameters after the kinematic fit.

IV. BACKGROUND SUBTRACTION

Main background sources for the process under study are the QED process $e^+e^- \to e^+e^-\gamma\gamma$, and multipion processes, e.g., $e^+e^- \to \pi^+\pi^-\pi^0\pi^0$. Events of these processes are strongly suppressed by our selection criteria and do not have a peak at the η mass in the two-photon invariant mass spectrum.

The only source of peaking background, the process $e^+e^- \to \eta K^+K^-$, is suppressed by the condition on $\chi^2_{\pi^+\pi^-\gamma\gamma}$. Its contribution estimated using Monte Carlo (MC) simulation and the $e^+e^- \to \eta K^+K^-$ cross section measured in Ref. [7] is found to be less than 0.15% and neglected.

To separate signal and background we fit to the two-photon invariant mass spectrum with a sum of signal and background distributions. The signal line shape is described by a double-Gaussian function, parameters of which are determined from a fit to the two-photon mass spectrum for simulated $e^+e^- \to \eta\pi^+\pi^-$ events. An example of such a fit at $\sqrt{s} = 1.5$ GeV is shown in Fig. 2.

To take into account a possible difference between data and simulation in the η peak position and two-photon mass resolution, we introduce two additional parameters, the mass shift ΔM ($m_{1,2} = m^{\rm MC}_{1,2} + \Delta M$) and a width correction $\Delta\sigma^2$ ($\sigma^2_{1,2} = (\sigma^{\rm MC}_{1,2})^2 + \Delta\sigma^2$), where $m^{\rm MC}_{1,2}$ and $\sigma^{\rm MC}_{1,2}$ are the means and σ's of the double-Gaussian function determined from simulation, and $m_{1,2}$ and $\sigma_{1,2}$ are the corrected values of these parameters.

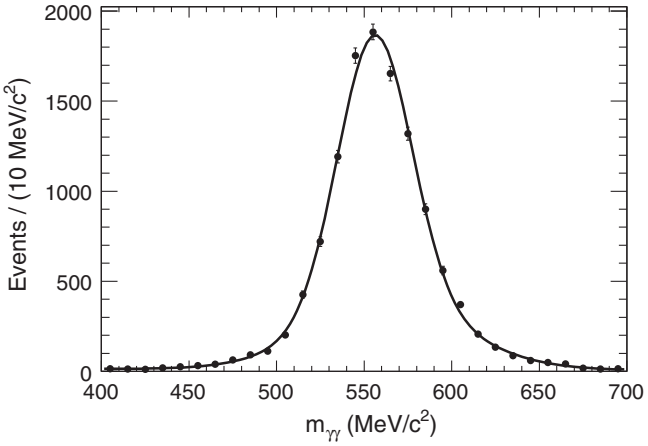

FIG. 2. The two-photon invariant-mass spectrum for simulated $e^+e^- \to \eta\pi^+\pi^-$ events at $\sqrt{s} = 1.5$ GeV (points with error bars) fitted with the double-Gaussian function.

The parameters $\Delta\sigma^2$ and ΔM are determined from the fit to the spectrum for data events from the energy interval near the maximum of the $e^+e^- \to \eta\pi^+\pi^-$ cross section ($\sqrt{s} = 1.45$–1.60 GeV). The spectrum and fitted curve are shown in Fig. 3. The nonpeaking background is described by a linear function. This assumption about the background shape was tested on simulated events of the dominant background process $e^+e^- \to \pi^+\pi^-\pi^0\pi^0$. The found values of correction parameters ($\Delta M = -3.0 \pm 0.9$ MeV$/c^2$ and $\Delta\sigma^2 = -89 \pm 33$ MeV$^2/c^4$ for the 2011 data set and $\Delta M = -1.5 \pm 1.5$ MeV$/c^2$ and $\Delta\sigma^2 = 104 \pm 65$ MeV$^2/c^4$ for the 2012 data set) and the assumption of linear background

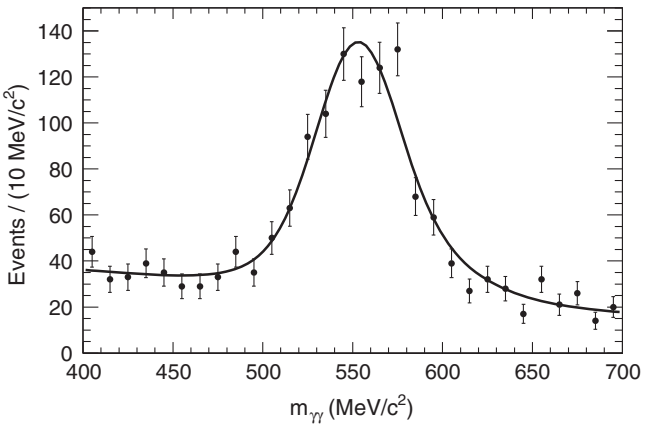

FIG. 3. The two-photon invariant-mass spectrum for data events selected in the energy range $\sqrt{s} = 1.45$–1.60 GeV. The curve is the result of the fit described in the text.

are used in the fits to data spectra for individual energy points. The difference between the correction parameters for 2011 and 2012 is due to difference in angular resolutions for charged tracks which is not taken into account in simulation.

The numbers of fitted $e^+e^- \to \eta\pi^+\pi^-$ events for different energy points are listed in Table II. We do not observe any excess of signal events over background at energies below 1.22 GeV.

The data mass spectra in the three energy regions, 1.20–1.45 GeV, 1.45–1.60 GeV, and 1.60–2.00 GeV, are also fit with a quadratic background. The difference between the fits with the two background hypotheses is taken as an estimate of the systematic uncertainty due to the unknown background shape. It is found to be 6.7% below 1.45 GeV, 1.0% in the energy range 1.45–1.60 GeV, and 2.2% above.

V. INTERNAL STRUCTURE OF THE $\eta\pi^+\pi^-$ FINAL STATE

The $\pi^+\pi^-$ invariant mass ($m_{\pi\pi}$) spectrum for $e^+e^- \to \eta\pi^+\pi^-$ data events from the energy range $\sqrt{s} =$ 1.45–1.60 GeV is shown in Fig. 4. The spectrum is obtained as a difference of the $\pi^+\pi^-$ mass spectrum for events with $500 < m_{\gamma\gamma} < 600$ MeV/c^2 and the spectrum for events from the sidebands ($400 < m_{\gamma\gamma} < 470$ MeV/c^2 and $630 < m_{\gamma\gamma} < 700$ MeV/c^2) divided by a scale factor of 1.4. The solid histogram in Fig. 4 is the result of MC simulation. The $e^+e^- \to \eta\pi^+\pi^-$ event generator is based on formulas for the differential cross section from Ref. [8] and uses the model of the $\eta\rho(770)$ intermediate state. The observed difference between data and MC spectra is too large to be explained by imperfect simulation of resolution effects, and may be a result of the contribution of other intermediate state, e.g., $\eta\rho(1450)$, and its interference with

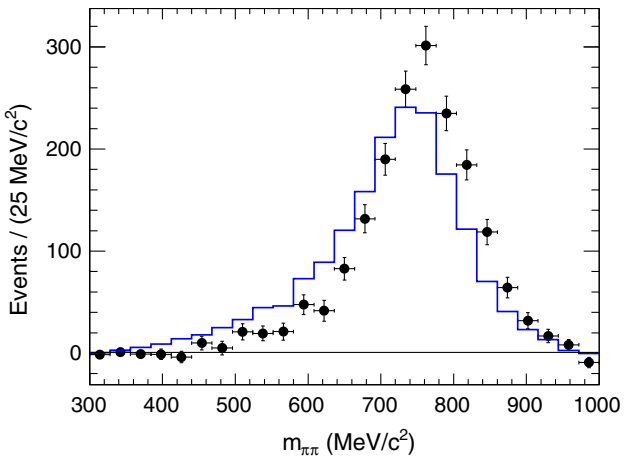

FIG. 4 (color online). The $\pi^+\pi^-$ invariant-mass spectrum for data (points with error bars) and simulated (histogram) $e^+e^- \to \eta\pi^+\pi^-$ events from the energy range $\sqrt{s} = 1.45$–1.60 GeV. The simulation uses a model of the $\eta\rho(770)$ intermediate state.

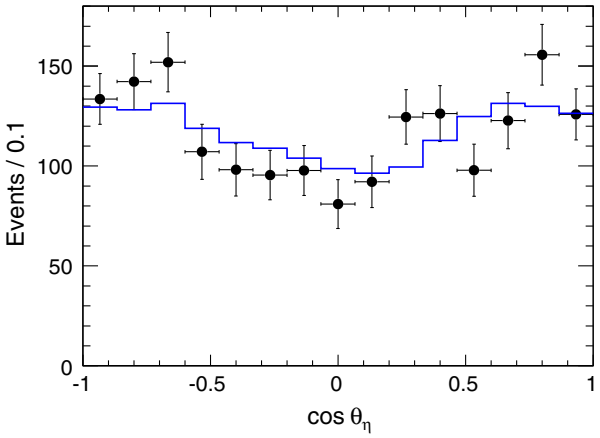

FIG. 5 (color online). The $\cos\theta_\eta$ distribution for data (points with error bars) and simulated (histogram) $e^+e^- \to \eta\pi^+\pi^-$ events from the energy range $\sqrt{s} = 1.45$–1.60 GeV. The simulation uses a model of the $\eta\rho(770)$ intermediate state.

the dominant $\eta\rho(770)$ amplitude. A similar effect was observed, for example, in the $J/\psi \to 3\pi$ decay [9], in which the Dalitz plot distribution deviates from the prediction for the $\rho\pi$ intermediate state.

In Fig. 5 we compare the data and simulated $\cos\theta_\eta$ distributions, where θ_η is the η-meson polar angle. In the $\eta\rho$ model this distribution is expected to be $1 + \cos^2\theta_\eta$. We see reasonable agreement between data and simulation in the angular distributions.

VI. DETECTION EFFICIENCY

The detection efficiency for the process under study is determined using MC simulation in the $\rho(770)\eta$ model. To estimate an influence of the deviation from this model observed in the previous section, we reweight simulation events according to the $m_{\pi\pi}$ spectrum observed in data. The shift in the detection efficiency, about 1%, is taken as an estimate of the model uncertainty associated with the $\rho(770)\eta$ assumption.

The simulation takes into account radiative corrections to the Born cross section calculated according to Ref. [10]. In particular, an extra photon emitted by initial particles is generated with the angular distribution modeled according to Ref. [11]. Such an approach requires knowledge of the energy dependence of the $e^+e^- \to \eta\pi^+\pi^-$ cross section. This dependence was taken initially from Ref. [4]. Then we repeat the simulation with the energy dependence measured in this work. The variation of the detection efficiency, less than 1.0% at $\sqrt{s} < 1.6$ GeV and less than 4.2% at higher energies, is considered as an estimate of the model error. The total model uncertainty of the detection efficiency is 1.4% at $\sqrt{s} < 1.6$ GeV and 4.3% at $\sqrt{s} > 1.6$ GeV.

Beam background overlapping with signal events can produce additional clusters in the calorimeter and tracks in the tracking system. To take into account this effect in MC

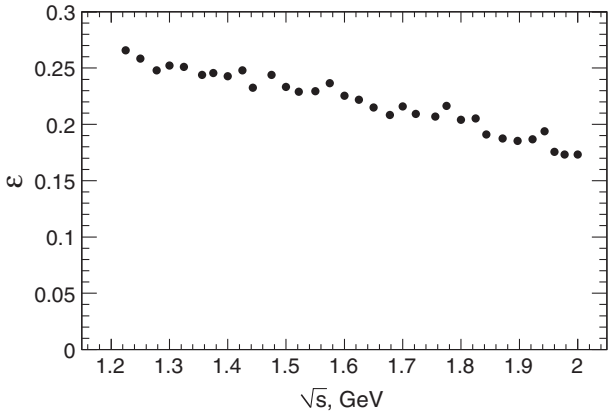

FIG. 6. The detection efficiency for simulated $e^+e^- \to \eta\pi^+\pi^-$, $\eta \to \gamma\gamma$ events.

simulation, beam-background events recorded during experiment with a special random trigger are merged with simulated events. The presence of beam-generated tracks and clusters in the calorimeter reduces detection efficiency, by about 10%.

The energy dependence of the detection efficiency is shown in Fig. 6. Nonmonotonic behavior of the efficiency as a function of energy is due to variations of experimental conditions (beam background, dead detector channels, etc.), which are taken into account in MC simulation.

The detection efficiency obtained using MC simulation is corrected to take into account a difference between data and simulation in detector response: $\varepsilon = \varepsilon_{\rm MC}(1-\Delta)$. To determine Δ, events from the energy region $\sqrt{s} =$ 1.45–1.60 GeV are used. We loosen a selection criterion, fit to $m_{\gamma\gamma}$ spectrum, and study variation in the fitted number of $e^+e^- \to \eta\pi^+\pi^-$ events in data and simulation. The efficiency correction for the tested criterion is determined from the data-MC simulation double ratio $\Delta = (N^*/N)_{\rm data}/(N^*/N)_{\rm MC} - 1$, where N and N^* are the fitted numbers of $e^+e^- \to \eta\pi^+\pi^-$ events selected with standard and loosened criteria.

To study the effect of the condition $N_\gamma = 2$, we perform a kinematic fit for events with more than two photons. From all possible two-photon combinations in an event we choose the combination with 400 MeV $\le m_{\gamma\gamma} \le$ 700 MeV and minimum $\chi^2_{\pi^+\pi^-\gamma\gamma}$. From the fit to the $m_{\gamma\gamma}$ spectrum for these events we determine $(N^* - N)$, and calculate the efficiency correction. To determine correction for the condition $N_c = 2$, we study events with $N_c = 3$. In the kinematic fit, two tracks with minimal r_i are used. For other selection criteria we shift the boundaries of the conditions, from 60 to 10000 for $\chi^2_{\pi^+\pi^-\gamma\gamma}$, from 200 to 10000 for χ^2_{vtx}, etc.

The resulting corrections are summarized in Table I. Listed are those conditions for which statistically significant deviations of the data-MC double ratios are observed. The two last rows in Table I represent corrections for the

TABLE I. The efficiency corrections.

	Δ, %
Condition $N_\gamma = 2$	-7.5 ± 2.3
Condition $N_c = 2$	2.0 ± 0.7
Condition $\chi^2_{\pi^+\pi^-\gamma\gamma} < 60$	-4.8 ± 3.0
Condition $\chi^2_{\rm vertex} < 200$	0.9 ± 0.4
Conditions $E_{\rm tot} < 0.9\sqrt{s}$ and $E_{\rm char} < 0.65\sqrt{s}$	-1.3 ± 0.6
Track reconstruction	0.3 ± 0.2
Photon conversion	0.4 ± 0.6
Total	-10.1 ± 3.9

TABLE II. The c.m. energy ($\sqrt{s}$), integrated luminosity (L), detection efficiency (ε), number of selected signal events (N), radiative-correction factor $(1+\delta)$, measured $e^+e^- \to \eta\pi^+\pi^-$ Born cross section (σ_B). For the number of events and cross section the statistical error is quoted. The systematic uncertainty on the cross section is 8.3% at $\sqrt{s} < 1.45$ GeV, 5.0% at $1.45 < \sqrt{s} < 1.60$ GeV, and 7.8% at $\sqrt{s} > 1.60$ GeV.

$\sqrt{s}$, GeV	σ_B, nb	N	ε	L, nb^{-1}	$1+\delta$
1.225	0.35 ± 0.15	20 ± 9	0.105	553	0.87
1.250	0.17 ± 0.15	8 ± 7	0.102	466	0.87
1.278	0.49 ± 0.13	56 ± 16	0.097	1225	0.87
1.300	0.50 ± 0.19	23 ± 10	0.099	484	0.87
1.325	0.74 ± 0.19	38 ± 10	0.099	542	0.86
1.356	1.07 ± 0.15	137 ± 21	0.096	1398	0.86
1.375	1.25 ± 0.22	70 ± 13	0.097	599	0.86
1.400	1.69 ± 0.24	100 ± 15	0.095	643	0.87
1.425	2.23 ± 0.25	125 ± 15	0.097	591	0.87
1.443	2.76 ± 0.19	355 ± 26	0.091	1442	0.88
1.475	3.31 ± 0.29	191 ± 18	0.096	608	0.89
1.500	3.63 ± 0.29	244 ± 20	0.092	731	0.90
1.522	4.47 ± 0.23	568 ± 30	0.090	1395	0.91
1.550	4.28 ± 0.33	225 ± 18	0.090	566	0.93
1.575	3.61 ± 0.36	154 ± 16	0.093	436	0.94
1.600	3.30 ± 0.34	139 ± 15	0.089	446	0.96
1.625	3.76 ± 0.34	189 ± 17	0.087	530	0.98
1.650	2.53 ± 0.32	116 ± 15	0.085	490	0.99
1.678	2.41 ± 0.19	290 ± 23	0.082	1314	1.01
1.700	2.79 ± 0.31	126 ± 14	0.085	472	1.01
1.723	2.05 ± 0.20	193 ± 19	0.082	1022	1.01
1.756	2.26 ± 0.19	249 ± 20	0.081	1198	1.02
1.775	1.97 ± 0.28	91 ± 13	0.085	473	1.03
1.800	2.09 ± 0.17	274 ± 22	0.080	1391	1.06
1.825	1.47 ± 0.24	74 ± 12	0.081	513	1.09
1.843	1.36 ± 0.15	173 ± 18	0.075	1369	1.11
1.871	0.94 ± 0.13	137 ± 18	0.074	1555	1.14
1.897	0.89 ± 0.11	171 ± 20	0.073	2033	1.17
1.922	0.81 ± 0.13	100 ± 15	0.073	1256	1.20
1.943	0.75 ± 0.12	102 ± 15	0.076	1312	1.22
1.960	0.76 ± 0.17	52 ± 11	0.069	724	1.24
1.978	0.81 ± 0.15	86 ± 14	0.068	1125	1.25
2.000	0.84 ± 0.21	47 ± 10	0.068	576	1.28

data-MC difference in the ratio of the charged-track reconstruction efficiency for pions and electrons [12], and in the probability of photon conversion in the material before the drift chamber [13].

The corrected values of the detection efficiency are listed in Table II. The statistical error on the detection efficiency is about 1%. So, the total uncertainty on the detection efficiency including the statistical error, the uncertainty in the efficiency correction, and the model uncertainty is 4.3% at $\sqrt{s} < 1.6$ GeV and 6.0% at $\sqrt{s} > 1.6$ GeV.

VII. LUMINOSITY MEASUREMENT

Integrated luminosity is determined using large-angle Bhabha scattering ($e^+e^- \to e^+e^-$) events selected with the following criteria:

(i) $N_c = 2$ (see the N_c definition in Sec. III);
(ii) $50° < \theta_{1,2} < 130°$, where $\theta_{1,2}$ are the polar angles of the charged particles;
(iii) $E_{1,2}/\sqrt{s} > 0.25$, $0.65 < (E_1 + E_2)/\sqrt{s} < 1.1$, where E_1 and E_2 are the energies of the charged particles measured in the calorimeter;
(iv) $|\Delta\theta| < 20°$, $|\Delta\phi| < 5°$, where $\Delta\theta$ and $\Delta\phi$ are the polar and azimuthal acollinearity angles.

To calculate the detection efficiency and the cross section for the large-angle Bhabha scattering, the BHWIDE [14] event generator is used. The integrated luminosity measured for each energy point (L_i) is listed in Table II. The theoretical uncertainty on the cross section calculation is better than 0.5%. The systematic uncertainty on the detection efficiency is estimated to be 2%.

VIII. RESULTS AND DISCUSSION

The Born cross section at the ith energy point is determined as

$$\sigma_{\rm B}^i = \frac{N_i}{\varepsilon_i L_i (1+\delta_i)}, \tag{1}$$

where δ_i is the radiative correction. Knowledge of the $e^+e^- \to \eta\pi^+\pi^-$ Born cross section at energies below $\sqrt{s_i}$ is required to calculate δ_i:

$$1 + \delta_i = \frac{\sigma_{\rm vis}(s_i)}{\sigma_{\rm B}(s_i)}, \tag{2}$$

$$\sigma_{\rm vis}(s) = \int_0^1 \sigma_{\rm B}(s(1-z))F(z,s)dz, \tag{3}$$

where $F(z,s)$ is a function describing the probability to emit extra photons with the total energy $z\sqrt{s}/2$ [10]. Technically, the radiative corrections are calculated using the VMD model for the Born cross section described below. Parameters of the model are determined from a fit with Eq. (3) to the measured visible cross section $N_i/(\varepsilon_i L_i)$. The obtained values of the radiative correction are listed in Table II. The model uncertainty on the radiative correction is estimated by variation of the model parameters within their errors and is found to be 0.6% below 1.45 GeV, 1.4% in the energy range 1.45–1.60 GeV, and 4.1% above 2.00 GeV.

The Born cross section for $e^+e^- \to \eta\pi^+\pi^-$ obtained using Eq. (1) is shown in Fig. 7 in comparison with the results of the most precise previous measurements by SND at VEPP-2M [5] and *BABAR* [4]. The numerical values are listed in Table II. The quoted errors on the cross section are statistical. The systematic uncertainty is 8.3% at $\sqrt{s} < 1.45$ GeV, 5.0% at $1.45 < \sqrt{s} < 1.60$ GeV, and 7.8% at $\sqrt{s} > 1.60$ GeV. It consists of the systematic uncertainty in background subtraction (Sec. IV), the uncertainty on the detection efficiency (Sec. VI), the model uncertainty on the radiative correction, and the error on the integrated luminosity (2%). It is seen that the data of all three experiments are in agreement.

The measured $e^+e^- \to \eta\pi^+\pi^-$ Born cross section is fitted using the VMD model with the three isovector states $\rho(770)$, $\rho(1450)$, and $\rho(1700)$ decaying to $\eta\rho(770)$ [8]:

$$\begin{aligned}
\sigma_{\rm B}(s) &= \int_{4m_\pi^2}^{(\sqrt{s}-m_\eta)^2} \frac{d\sigma}{dq^2} dq^2, \\
\frac{d\sigma}{dq^2}(s,q^2) &= \frac{4\alpha^2}{3}\frac{1}{s\sqrt{s}} \frac{\sqrt{q^2}\Gamma_\rho(q^2)P_\eta^3(s,q^2)}{(q^2-m_\rho^2)^2 + (\sqrt{q^2}\Gamma_\rho(q^2))^2}|F(s)|^2, \\
P_\eta^2(s,q^2) &= [(s-m_\eta^2-q^2)^2 - 4m_\eta^2 q^2]/4s, \\
\Gamma_\rho(q^2) &= \Gamma_\rho(m_\rho^2)\frac{m_\rho^2}{q^2}\left(\frac{p_\pi^2(q^2)}{p_\pi^2(m_\rho^2)}\right)^{\frac{3}{2}}, \\
p_\pi^2(q^2) &= q^2/4 - m_\pi^2,
\end{aligned} \tag{4}$$

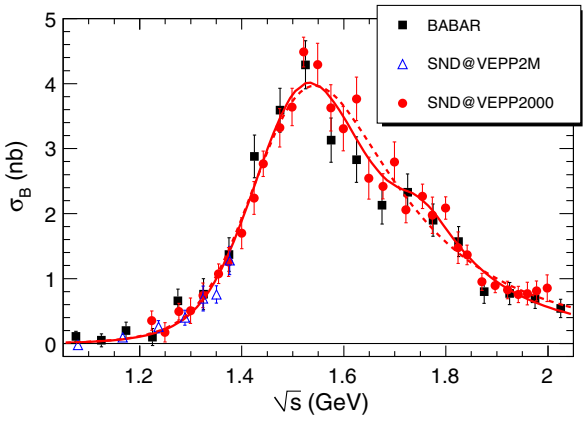

FIG. 7 (color online). The Born cross section for $e^+e^- \to \eta\pi^+\pi^-$ measured in this (SND@VEPP2000) and previous experiments (*BABAR* [4] and SND@VEPP2M [5]). The solid curve is the result of the VMD fit with the $\rho(770)$, $\rho(1450)$ and $\rho(1700)$ resonances. The dashed curve is the same fit without the $\rho(1700)$ contribution.

where q is the 4-momentum of the $\pi^+\pi^-$ system, and $F(s)$ is the transition form factor for the vertex $\gamma^* \to \eta\rho$:

$$F(s) = \sum_V \frac{m_V^2}{g_{V\gamma}} \frac{g_{V\rho\eta}}{s - m_V^2 + i\sqrt{s}\Gamma_V(s)},$$
$$V = \rho(770), \rho(1450), \rho(1700). \quad (5)$$

Here $g_{V\rho\eta}$ and $g_{V\gamma}$ are the coupling constants for the transitions $V \to \rho\eta$ and $V \to \gamma^*$, respectively. It is convenient to use notation $g_{V\rho\eta}/g_{V\gamma} = g_V e^{i\phi_V}$.

In the fit, the mass and width of the $\rho(770)$ resonance are fixed at their nominal values [15]. The phase $\phi_{\rho(770)}$ is set to 0. The coupling constants $|g_{\rho\rho\eta}|$ and $|g_{\rho\gamma}|$ are calculated using data on the partial widths for the decays $\rho(770) \to e^+e^-$ and $\eta\gamma$ [15]:

$$g_{\rho\gamma}^2 = \frac{4\pi}{3}\alpha^2 \frac{m_\rho}{\Gamma(\rho \to e^+e^-)},$$
$$g_{\rho\eta\gamma}^2 = \frac{24}{\alpha} m_\rho^3 \frac{\Gamma(\rho \to \eta\gamma)}{(m_V^2 - m_\eta^2)^3},$$
$$g_{\rho\rho\eta} = g_{\rho\gamma} g_{\rho\eta\gamma}. \quad (6)$$

For the $\rho(1450)$ and $\rho(1700)$ resonances, the masses and widths are also fixed at the nominal values [15], but are allowed to be varied within their errors. The ratios $g_{\rho(1450)}$ and $g_{\rho(1700)}$ are free fit parameters. Since the coupling constants are not expected to have sizable imaginary parts, the fit is performed assuming that the phases $\phi_{\rho(1450)}$ and $\phi_{\rho(1700)}$ are equal to zero or π. The best value of $\chi^2/\nu = 37/31$ ($P(\chi^2) \approx 20\%$), where ν is the number of degrees of freedom, is obtained for the phase combination $\phi_{\rho(1450)} = \phi_{\rho(1700)} = \pi$. The fitted ratios of the coupling constants are

$$g_{\rho(1450)} = 0.48^{+0.05}_{-0.06}\ \text{GeV}^{-1},$$
$$g_{\rho(1700)} = 0.02^{+0.03}_{-0.01}\ \text{GeV}^{-1}. \quad (7)$$

The fit result is shown in Fig. 7. The obtained value of $g_{\rho(1700)}$ deviates from zero by only 2σ. So, we cannot draw a definite conclusion that the $\rho(1700)$ contribution is needed for data description. For comparison, we show in Fig. 7 the result of the fit with $g_{\rho(1700)} = 0$. The χ^2/ν value for this fit is 42.6/32 ($P(\chi^2) \approx 10\%$). The value of $g_{\rho(1450)}$ is used to obtain the product of the branching fractions,

$$B(\rho(1450) \to \eta\pi^+\pi^-)B(\rho(1450) \to e^+e^-)$$
$$= (4.3^{+1.1}_{-0.9} \pm 0.2) \times 10^{-7}, \quad (8)$$

where the second error is systematic. This result can be compared with the same products for other $\rho(1450)$ decays: $B(\rho(1450) \to \omega\pi)B(\rho(1450) \to e^+e^-) = (5.3 \pm 0.4) \times 10^{-6}$ [13] and $B(\rho(1450) \to \pi^+\pi^-)B(\rho(1450) \to e^+e^-) = (5.6 \pm 1.8) \times 10^{-7}$. The later product is calculated using the parameters of the VMD fit to the $e^+e^- \to \pi^+\pi^-$ cross section performed in Ref. [16]. We obtain the following ratios of the branching fractions:

$$B(\rho(1450) \to \omega\pi) : B(\rho(1450) \to \eta\pi^+\pi^-) :$$
$$B(\rho(1450) \to \pi^+\pi^-) = 12.3 \pm 3.1 : 1 : 1.3 \pm 0.4. \quad (9)$$

There are several theoretical predictions for these ratios, for example, 8.1 : 1 : 9.5 [17] and 6.4 : 1 : 3.8 [18]. It is seen that the experimental ratio $B(\rho(1450) \to \omega\pi)/B(\rho(1450) \to \eta\pi^+\pi^-)$ is in reasonable agreement with the predictions, while the $\rho(1450) \to \pi^+\pi^-$ decay rate is too small compared to the theoretical expectations.

Under the CVC hypothesis, our data on the $e^+e^- \to \eta\pi^+\pi^-$ cross section can be used to calculate the branching fraction of the $\tau^- \to \eta\pi^-\pi^0\nu_\tau$ decay [19],

$$\frac{B(\tau^- \to \eta\pi^-\pi^0\nu_\tau)}{B(\tau^- \to \nu_\tau e^-\bar{\nu}_e)}$$
$$= \frac{3\cos^2\theta_c}{2\pi\alpha^2 m_\tau^8} \int_0^{m_\tau^2} dq^2 q^2 (m_\tau^2 - q^2)^2$$
$$\times (m_\tau^2 + 2q^2)\sigma_{e^+e^- \to \eta\pi^+\pi^-}(q^2). \quad (10)$$

Performing numerical integration of the measured cross section, we obtain the branching fraction,

$$B(\tau^- \to \eta\pi^-\pi^0\nu_\tau) = (0.156 \pm 0.004 \pm 0.010)\%, \quad (11)$$

which is in agreement with the world average experimental value $(0.139 \pm 0.010)\%$ [15] and with the CVC result $(0.153 \pm 0.018)\%$ [20] obtained using earlier $e^+e^- \to \eta\pi^+\pi^-$ data.

IX. SUMMARY

In this paper the cross section for $e^+e^- \to \eta\pi^+\pi^-$ has been measured in the c.m. energy range from 1.22 to 2.00 GeV. Our data are in agreement with previous measurements and most precise in the energy region between 1.4 and 2.0 GeV.

We have studied the internal structure of the $\eta\pi^+\pi^-$ final state. It has been found that the $\rho(770)\eta$ intermediate state is dominant, but does not fully describe the observed $\pi^+\pi^-$ invariant mass spectrum.

The measured cross section is well described by the VMD model with the $\rho(770)$ and $\rho(1450)$ resonances. Adding the $\rho(1700)$ contribution improves the fit quality, but is not necessary at the current level of statistics. From the fit we have extracted the product of the branching fractions $B(\rho(1450) \to \eta\pi^+\pi^-)B(\rho(1450) \to e^+e^-)$ and compared it with the same products for $\rho(1450) \to \omega\pi^0$ and $\rho(1450) \to \pi^+\pi^-$ decays.

The branching fraction of $\tau^- \to \eta\pi^-\pi^0\nu_\tau$ decay has been calculated from our cross-section data under the CVC hypothesis. The obtained $B(\tau^- \to \eta\pi^-\pi^0\nu_\tau)$ value is in agreement with the current experimental value and has comparable accuracy. The CVC hypothesis for the $\eta\pi\pi$ system works within the experimental accuracy of about 10%.

ACKNOWLEDGMENTS

This work is partially supported in the framework of the State order of the Russian Ministry of Science and Education, by RFBR Grants No. 12-02-01250-a, 14-02-31375-mol_a, 13-02-00375 and the Russian Federation Presidential Grant for Scientific Schools NSh-2479.2014.2.

[1] V. P. Druzhinin *et al.* (ND Collaboration), Phys. Lett. **174B**, 115 (1986).
[2] A. Antonelli *et al.* (DM2 Collaboration), Phys. Lett. B **212**, 133 (1988).
[3] R. R. Akhmetshin *et al.* (CMD-2 Collaboration), Phys. Lett. B **489**, 125 (2000)
[4] B. Aubert *et al.* (*BABAR* Collaboration), Phys. Rev. D **76**, 092005 (2007); **77**, 119902(E) (2008).
[5] M. N. Achasov *et al.* (SND Collaboration) JETP Lett. **92**, 80 (2010).
[6] Yu. M. Shatunov *et al.*, in *Proceedings of the 7th European Particle Accelerator Conference, Vienna, 2000* (EPS, Geneva, 2000), p. 439 [http://accelconf.web.cern.ch/AccelConf/e00/PAPERS/MOP4A08.pdf].
[7] B. Aubert *et al.* (*BABAR* Collaboration), Phys. Rev. D **77**, 092002 (2008).
[8] N. N. Achasov and V. A. Karnakov, Pis'ma Zh. Eksp. Teor. Fiz. **39**, 285 (1984) [JETP Lett. **39**, 342 (1984)].
[9] B. Aubert *et al.* (*BABAR* Collaboration), Phys. Rev. D **70**, 072004 (2004).
[10] E. A. Kuraev and V. S. Fadin, Yad. Fiz. **41**, 733 (1985) [Sov. J. Nucl. Phys. **41**, 466 (1985)].
[11] G. Bonneau and F. Martin, Nucl. Phys. **B27**, 381 (1971).
[12] M. N. Achasov *et al.* (SND Collaboration), J. Exp. Theor. Phys. **101**, 1053 (2005).
[13] M. N. Achasov *et al.* (SND Collaboration), Phys. Rev. D **88**, 054013 (2013).
[14] S. Jadach, W. Placzek, and B. F. L. Ward, Phys. Lett. B **390**, 298 (1997).
[15] K. A. Olive *et al.* (Particle Data Group), Chin. Phys. C **38**, 090001 (2014).
[16] J. P. Lees *et al.* (*BABAR* Collaboration), Phys. Rev. D **86**, 032013 (2012).
[17] S. Godfrey and N. Isgur, Phys. Rev. D **32**, 189 (1985).
[18] A. Donnachie and Yu. S. Kalashnikova, Phys. Rev. D **60**, 114011 (1999).
[19] F. J. Gilman, Phys. Rev. D **35**, 3541 (1987).
[20] V. Cherepanov and S. Eidelman, Nucl. Phys. B, Proc. Suppl. **218**, 231 (2011).